Structure of Rutile TiO_2 (110)-(1 × 2): Formation of Ti_2O_3 Quasi-1D Metallic Chains

M. Blanco-Rey, J. Abad, C. Rogero, J. Mendez, M. F. Lopez, J. A. Martin-Gago, and P. L. de Andres
Instituto de Ciencia de Materiales (CSIC), Cantoblanco, 28049 Madrid, Spain
(Received 8 November 2005; published 6 February 2006)

Combining STM, LEED, and density functional theory, we determine the atomic surface structure of rutile TiO_2 (110)-(1 × 2): nonstoichiometric Ti_2O_3 stripes along the [001] direction. LEED patterns are sharp and free of streaks, while STM images show monatomic steps, wide terraces, and no cross-links. At room temperature, atoms in the Ti_2O_3 group have large amplitudes of vibration. The long quasi-1D chains display metallic character, show no interaction between them, and cannot couple to bulk or surface states in the gap region, forming good atomic wires.

DOI: 10.1103/PhysRevLett.96.055502 PACS numbers: 68.35.Bs, 61.14.Hg, 68.47.Gh, 73.90.+f

A better understanding of metal oxide surfaces will certainly make a huge impact on technologically important fields like heterogeneous catalysis, photochemistry, gas sensing, anticorrosion coatings, etc. [1]. Metal oxides, and in particular TiO_2, are the most extensively used support in catalytic devices. To design new catalysts, or to improve existing ones, a full description of their structural and electronic properties is necessary. The (110) face of TiO_2 makes a paradigmatic example as its most stable face and is known to host interesting surface chemistry. However, only recently has the geometrical disposition of atoms on the 1 × 1 surface been quantitatively determined by full dynamical low-energy electron diffraction (LEED) work [2]. Upon annealing, this face is reduced and results in a 1 × 2 reconstruction. Several models for this reconstruction have been proposed to explain qualitatively the STM images [Fig. 2(b) below], but these models have differed even on the surface stoichiometry, e.g., (i) Ti_2O_3 "added row" [3], (ii) "missing row" [4], (iii) "missing unit" [5], etc. In this work, we combine scanning tunneling microscopy (STM), full dynamical LEED, and density functional theory (DFT) to get a quantitative structural determination of the 1 × 2 reconstruction on (110) rutile TiO_2. The structure shows the existence of long nonstoichoimetric Ti_2O_3 added rows, in agreement with Onishi's model [3] (Fig. 1). The chemisorption energy for one of those Ti_2O_3 groups is 5.4 eV per unit cell, very similar to the bonding interaction between Ti_2O_3 and TiO_2 (6.3 eV), and it is useful to visualize the group as an adsorbed molecule producing long quasi-one-dimensional strips on the surface (Fig. 2). Most interesting, these quasi-1D molecular wires have a metallic character, making an ideal system to carry experiments to study 1D conductance. The outer oxygen on the Ti_2O_3 group [labeled O(1) in Fig. 1] have an unusual large rms vibration amplitude (about 0.36 Å), related to a relatively flat potential region around these positions. It is worth noticing the buckling in the trough: Ti(d) and O(5) are separated by a vertical distance of 0.46 Å. Finally, while typical Ti-Ti distances in bulk are 3.56 Å, we find that both Ti(b) and Ti(c) are attracted to Ti(a), to distances of 3.36 and 3.44 Å.

Experiments have been performed at room temperature on a TiO_2 rutile single crystal (PI-KEM Ltd., UK), treated by cycles for Ar^+ ion bombardment (1 keV, 10–30 min) under ultrahigh vacuum conditions (base pressure 2×10^{-10} mbar). The absence of contaminants has been judged by Auger electron spectroscopy. Annealing conditions have been carefully investigated to get a well characterized reconstruction (1150 K, 60 min). This procedure gives a very sharp 1 × 2 LEED pattern, with low background. STM images were recorded *in situ* at constant current mode and room temperature. Tungsten tips were prepared by field emission. Prolonged electron beam exposure during the LEED $I(V)$ measurements produces degradation of the LEED spots and increasing background intensity. To avoid these effects, the sample was displaced at short time intervals to expose fresh areas to the electron beam, and the sample was reannealed (1150 K, 10–30 min) to restore the 1 × 2 pattern to the initial quality. $I(V)$ curves have been measured at normal and off-normal incidence to increase the accuracy of the structural analysis. Figure 2(a) shows a STM representative image. We

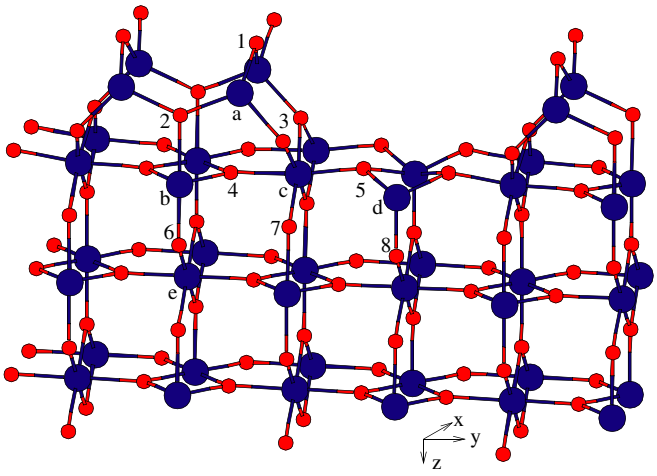

FIG. 1 (color online). Model for 1 × 2 TiO_2 (110) (best fit to LEED, $R_P = 0.28$). Large and small spheres represent Ti(a–e) and O(1–8) atoms, respectively. The lowest layer has been frozen to optimized bulklike positions.

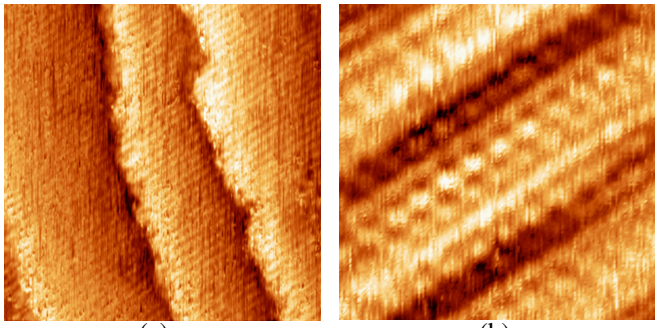

FIG. 2 (color online). Constant current STM images of 1×2 TiO_2 (110), $V = +1.5$ V. (a) Monatomic steps and large terraces on a 500×500 Å^2 area ($I = 0.146$ nA). (b) A high-resolution image on a 30×30 Å^2 area ($I = 0.178$ nA).

observe monatomic steps of 3.2 ± 0.2 Å, bright stripes separated by 13 ± 1 Å, and large terraces more than 100 Å wide, while "cross-links" are not present [6]. Even in high-resolution images [Fig. 2(b)], individual atomic positions, or even the composition, cannot be easily determined.

To obtain quantitative information about the stoichiometry and the atomic positions LEED $I(V)$ curves for different diffracted beams, $I_{\vec{g}}(E)$, have been compared with theoretical intensities computed for different trial models [7]. Nineteen atoms have been systematically included in the search, including both geometrical and vibrational variables. To explore more effectively this enormous parameter space tensor LEED, layer doubling and composite layer techniques have been used [8]. The theoretical and experimental curves are quantitatively compared with the Pendry R factor, R_P [9]. Phase shifts ($l_{max} = 8$) have been computed from MUFPOT and Hartree-Fock solutions to the neutral and ionic atomic species [10]. By analyzing the charge density distribution on a TiO_2 molecule [11], we determine muffin-tin radii equal for both species (0.95 Å). Pendry R factors larger than 0.5 reflect such a poor correlation between experiment and theory that those models can immediately be rejected. This is the case for most of the candidates that have been rejected from an initial screening performed only with the normal incidence data. In particular, we have the following: (1) the Ti_3O_6 groups [12] with $R_P = 0.67$, (2) the Ti_3O_5 groups [5] with $R_P = 0.61$, and (3) the missing-row model [13] with $R_P = 0.52$, etc. We focus on the only model showing a reasonable agreement: the Ti_2O_3 added row proposed by Onishi and Iwasawa [3], with $R_P = 0.28$ (see Fig. 1). Different reasonable deformations of this model have been explored, particularly the interstitial position for Ti(a) [14]. All these possibilities resulted in $R_P \geq 0.5$. We notice that in order to get a reasonable fit, it is important to pay attention to parameters related to atomic vibrations. R_P drops from ≈ 0.4 to ≈ 0.3 after we introduce the effect of isotropic vibrations through a Debye-Waller model. In Table I we analyze our results from the point of view of both data sets and the integer and noninteger beams, respectively. The global value of $R_P = 0.28$ is very convincing, as it is the visual agreement between experimental and calculated beams (Fig. 3). Furthermore, R factors for the different data sets show a reassuring similar agreement.

TABLE I. Pendry R factors for best-fit Ti_2O_3 "added-row" structure (overlap between experiment and theory is given in eV). Optimized values for the real and imaginary parts of the self-energy are 8.0 and 5.5 eV, respectively.

	Normal incidence	Off-normal incidence	All
Integer beams	0.27 (790 eV)	0.22 (915 eV)	0.25
Noninteger beams	0.30 (634 eV)	0.38 (612 eV)	0.33
All beams	0.28 (1424 eV)	0.28 (1527 eV)	0.28

The consistency of the structure can be tested further by comparing with "*ab initio*" DFT calculations. Electronic states have been expanded in a plane-wave basis [15] or in Gaussians [11], and appropriated pseudopotentials [16] have been used to describe the different atoms (O $2s^2$ $2p^4$ and Ti $3s^2$ $3p^6$ $3d^2$ $4s^2$). The Perdew-Burke-Ernzerhof generalized gradient approximation to the exchange and correlation functional has been used for plane waves [17], and Becke's B3LYP for Gaussians [18]. For plane waves, we have used an energy cutoff of 400 eV with finite basis corrections estimated at ± 5 eV increments, while for Gaussians we have used cc-pVTZ for oxygen, and SDD for Ti. The supercell for the 1×2 model included 41 atoms with the lowest layer kept fixed to optimized bulk positions (see Fig. 1). This makes a slab with three 1×1 layers and one 1×2 layer (approximately

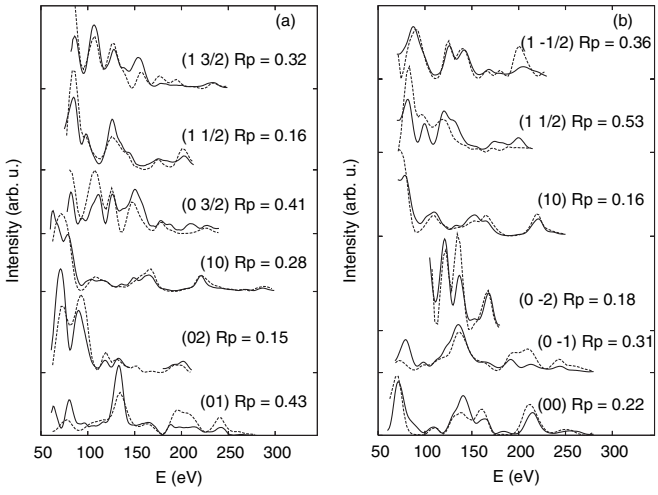

FIG. 3. Experimental LEED $I_{\vec{g}}(E)$ curves (full line) compared with theoretical calculations (dashed line) for the best-fit model. A few representative integer and noninteger beams are given for (a) normal incidence and (b) off-normal one ($\theta = 4° \pm 1°$ and $\phi = 25° \pm 10°$).

13 Å wide). To avoid interactions between different slabs, we have introduced a 24 Å vacuum gap in the direction perpendicular to the surface. Calculations were performed with a $7 \times 13 \times 1$ Monkhorst and Pack k-points grid ($4 \times 7 \times 4$ for bulk calculations). Convergence on the energy cutoff and the number of k points have been monitored to make sure that the maximum change in any atomic position is ≤ 0.03 Å. Normal modes for the Ti_2O_3 group were computed with GAUSSIAN, while phonons were estimated only at the Γ point, constructing the dynamical matrix from small finite displacements of each atom in the unit cell (0.005 Å). Spin-polarized calculations starting from different initial total spin configurations have been performed: for this structure, however, energy differences are small (≤ 0.1 eV), and the spin-paired solution is the preferred one. Other convergence thresholds are total energy change per ion $\leq 10^{-5}$ eV, maximum ion displacement ≤ 0.001 Å, maximum force ≤ 0.01 eV Å^{-1}, and maximum stress on the unit cell ≤ 0.02 GPa.

Using a plane-waves basis, we minimize the total energy and the stress on the unit cell [15]. This approach gives correctly the lattice parameters for bulk TiO_2: $a = 4.674$ Å and $c = 2.994$ Å (about 1.6% and 0.5% bigger than the experimental values). The material has an important ionic character, with charges on O and Ti of -0.65 and 1.29 electrons, respectively (derived from a Mulliken analysis). On the TiO_2 molecule these values are -0.53 and 1.1, respectively. Spin-polarized calculations performed with the same precision do not result in lower total energies. The computed band gap is 2.2 eV (0.8 too short compared with the experimental value). The band structure for the bulk rutile, and the corresponding density of states agree well with previous calculations [19]. Next, we proceed to minimize the total energy and the stress on the 1×2 surface reconstruction. We compare LEED and DFT results in Table II. Atomic positions agree well between both approaches when the error bars are taken into account. The maximum discrepancy on a perpendicular distance is 0.19 Å for O(2). Indeed, there are only two atoms where we find discrepancies outside the error bars: O(2) and Ti(d). However, because the DFT analysis is strictly performed at $T = 0$ K, they could be reconciled by taking into account their large amplitudes of vibration. We notice that O(1) displays an unusually large vibration amplitude, too, and its associated uncertainty in z is large; this atom is discussed in more detail below. From the point of view of surface chemistry, it is interesting to compare different bond lengths between atoms: Ti(a)-Ti(b) and Ti(a)-Ti(c) bond lengths are reduced with respect to the typical Ti-Ti bulk distance (3.56 Å + 0.04 Å for DFT) by 0.2 and 0.12 Å, respectively. The maximum discrepancy between LEED and DFT on these values is 0.04 Å: both techniques show the existence of an increased interaction between these Ti atoms. Regarding the interaction between Ti and O, the highest reduction in bond length is observed between Ti(d) and O(8): 1.77 Å (discrepancy with DFT is 0.04 Å), making this fivefold coordinated Ti interesting from the point of view of chemical reactivity. We have analyzed 19 relevant bond lengths in the surface region: the average discrepancy between LEED and DFT is less than 0.001 Å, with a standard deviation of 0.05 Å. From these 19 lengths, five have differences between LEED and DFT bigger than 0.05 Å: Ti(b)-O(2) ($+0.13$), Ti(a)-O(1) (-0.10), Ti(a)-O(2) (-0.064), Ti(a)-O(3) (-0.067), and Ti(b)-O(6) ($+0.061$). The position for O(1) merits some discussion on its own: our LEED analysis shows a second minimum in the R factor where the Ti(a)-O(1) bond length is reduced to 1.58 Å. These two minima yield nearly equal R factors, and we cannot choose one of the associated structures from the LEED analysis alone. Such a short bond length could be reconciled with a double bond and atop adsorption [e.g., the (011) 2×1 [20]], but R factors related to atop adsorption are too high ($R_P \geq 0.5$). The discrepancy with DFT for this second position would increase to $+0.22$ Å, and we favor the first one. It is interesting to notice that the total energy increases slowly as a function of the height of O(1), explaining why large amplitudes of vibration can be found, giving a rather delocalized picture of the atom, and a large uncertainty on the position derived from LEED (see Table II). We find that a vertical displacement of the two oxygen atom in the unit cell towards the bulk by about 0.27 Å brings an increase in the total energy of about 0.15 eV, while a small displacement towards the vacuum region brings restoring forces 4 times bigger. The group Ti_2O_3 adsorbed on the surface shows vibrational modes on a band from 50 to 500 cm^{-1}. These soft modes (e.g., 50 cm^{-1}) correspond to semiclassical amplitudes of vibration of ≈ 0.35 Å, which is the order of magnitude we obtain from LEED. We have tried to

TABLE II. Comparison between LEED and DFT structures. Cartesian coordinates x, y, z, root mean square vibration amplitude, u, and DFT displacement respect the LEED value in the perpendicular, Δz, and parallel directions, Δy, are given in Å. Error bars are given for z. Charge variation with respect to bulk, ΔQ, is given in units of the electron charge.

Atom	u	x	y	z	Δz	Δy	ΔQ
Ti(a)	0.22	1.48	1.77	-5.99 ± 0.03	-0.02	0.00	0.04
Ti(b)	0.14	1.48	0.00	-3.14 ± 0.07	-0.06	0.00	0.02
Ti(c)	0.14	0.00	3.28	-3.27 ± 0.06	-0.05	0.01	-0.03
Ti(d)	0.14	1.48	6.49	-3.08 ± 0.05	-0.14	0.00	-0.05
O(1)	0.36	0.00	1.99	-7.16 ± 0.24	0.15	0.00	0.00
O(2)	0.14	1.48	0.00	-5.23 ± 0.07	-0.19	0.00	-0.06
O(3)	0.12	1.48	3.07	-4.60 ± 0.11	-0.12	0.00	-0.05
O(4)	0.10	0.00	1.25	-3.21 ± 0.12	-0.15	0.01	-0.04
O(5)	0.10	0.00	5.22	-3.54 ± 0.06	-0.05	0.02	-0.06
O(6)	0.10	1.48	0.00	-1.30 ± 0.22	0.0	0.00	-0.02
O(7)	0.10	1.48	3.28	-2.03 ± 0.22	-0.10	0.04	-0.02
O(8)	0.10	1.48	6.49	-1.31 ± 0.12	-0.09	0.00	-0.01

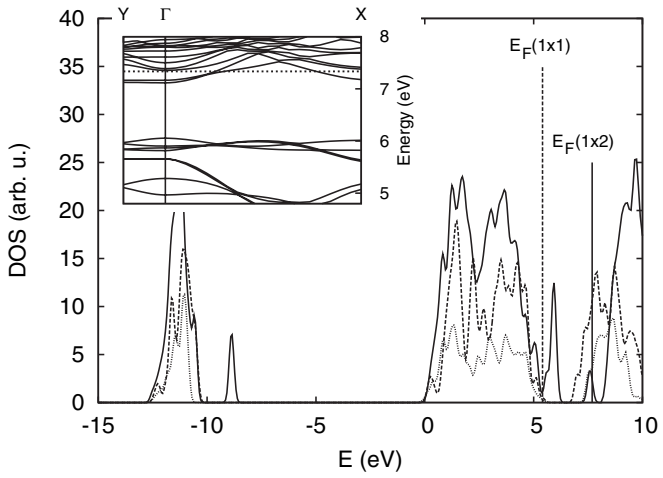

FIG. 4. Density of states for the 1×2 TiO_2 (110) (solid line) compared with 1×1 TiO_2 (110) (dashed line), and bulk rutile TiO_2 (dotted line). Fermi energies are marked by vertical lines for bulk, the 1×1 (5.4 eV), and the 1×2 (7.5 eV). Alignment of peaks near -27.7 eV has been used to compensate the dipole, resulting in good alignment of peaks near -51.5 and -11.0 eV. Inset: band structure for 1×2 TiO_2 (110) along Γ-X and Γ-Y.

refine the LEED calculations by including anisotropic vibrations of the topmost oxygen atoms, but the R factor did not improve significantly. This result could be understood if several different modes are relevant at the same time, resulting in a fairly isotropic average of displacements. Finally, we should mention that a different group working with LEED and surface x-ray diffraction on this reconstruction has reported preliminary results favoring the same Ti_2O_3 stoichiometry [21].

It is most interesting to compare the density of states of the 1×1 surface and the bulk rutile to the one found on the nonstoichiometric 1×2 slab. Figure 4 shows the appearance of new peaks associated with the Ti_2O_3 groups. More importantly, states associated with the reconstruction appear in the gap: the Fermi energy is located now about 2 eV above the edge of the valence band (the surface is reduced with respect to the 1×1 surface), in the middle of a small peak in the bulk gap region. This feature comes from Ti(a) $3d$ orbitals, sitting on a local reduced environment, and results in a metallic character related to the bands crossing the Fermi level in the direction $\Gamma - X$. Therefore, this peak has a similar origin to the Ti^{+3} states caused by O vacancies on the reduced TiO_2(110) surface, being the main difference their strong anisotropy related to the 1×2 reconstruction. From an experimental point of view, it helps to explain why the surface is not appreciably charged during the LEED experiment, and might be related to a small peak observed in ultraviolet photoelectron spectroscopy and x-ray photoelectron spectroscopy [22]. We note that the existence of this peak is not enough to prove the existence of the predicted quasi-1D state: angular resolved experiments would be needed to measure the peak dispersion. The implication is that the long Ti_2O_3 chains may behave as ideal long conducting wires. They cannot couple to other (nonexisting) surface or bulk states, and do not interact between them. Indeed, bands crossing the Fermi energy along the $\Gamma - X$ direction show a nice parabolic dispersion, while in the perpendicular one, Γ-Y, bands are rather flat supporting the absence of chain-chain coupling (inset of Fig. 4).

This work has been financed by the CICYT (Spain) under Contract No. MAT2002-395; M. B. R. gratefully acknowledges financial support from MEC (Spain). Computing resources have been contributed by the Barcelona Supercomputer Centre (http://www.bsc.es), and the CTI (CSIC). We are grateful to R. Lindsay, A. Wander, and G. Thornton for very useful discussion.

[1] U. Diebold, Surf. Sci. Rep. **48**, 53 (2003).
[2] R. Lindsay *et al.*, Phys. Rev. Lett. **94**, 246102 (2005).
[3] H. Onishi and Y. Iwasawa, Surf. Sci. Lett. **313**, L783 (1994).
[4] P. Moller and M. Wu, Surf. Sci. **224**, 265 (1989).
[5] C. Pang *et al.*, Phys. Rev. B **58**, 1586 (1998).
[6] R. Bennett, P. Stone, and M. Bowker, Faraday Discuss. **114**, 267 (1999).
[7] M. V. Hove, W. Weinberg, and C. Chan, *Low-Energy Electron Diffraction* (Springer, Berlin, 1986).
[8] V. Blum and K. Heinz, Comput. Phys. Commun. **134**, 392 (2001).
[9] J. Pendry, J. Phys. C **13**, 937 (1980).
[10] J. Pendry, *Low-Energy Electron Diffraction* (Academic, London, 1974).
[11] M. Frisch *et al.*, GAUSSIAN 03, revision b.05, http://www.gaussian.com.
[12] R. Bennett, P. Stone, and M. Bowker, Phys. Rev. Lett. **82**, 3831 (1999).
[13] P. Murray, N. Condon, and G. Thornton, Phys. Rev. B **51**, 10 989 (1995).
[14] S. Elliott and S. Bates, Phys. Chem. Chem. Phys. **3**, 1954 (2001).
[15] M. Segall *et al.*, J. Phys. Condens. Matter **14**, 2717 (2002); http://www.accelrys.com.
[16] D. Vanderbilt, Phys. Rev. B **41**, 7892 (1990).
[17] J. Perdew, K. Burke, and M. Ernzerhof, Phys. Rev. Lett. **77**, 3865 (1996).
[18] A. Becke, J. Chem. Phys. **98**, 1372 (1993).
[19] P. Sorantin and K. Schwartz, Inorg. Chem. **31**, 567 (1992).
[20] T. Beck *et al.*, Phys. Rev. Lett. **93**, 036104 (2004).
[21] R. Lindsay *et al.*, ASEVA Summer School, Avila, Spain, 2005.
[22] J. Abad *et al.*, Appl. Surf. Sci. **234**, 497 (2004).